Nonlocal density-functional calculations of the surface electronic structure of metals: Application to aluminum and palladium

M. Heinrichsmeier, A. Fleszar, and W. Hanke
Institut für Theoretische Physik, Universität Würzburg, Am Hubland, D-97074 Würzburg, Germany

A. G. Eguiluz
Department of Physics and Astronomy, The University of Tennessee, Knoxville, Tennessee 37996-1200 and Solid State Division, Oak Ridge National Laboratory, Oak Ridge, Tennessee 37831-6032

(Received 23 December 1997)

We report density-functional calculations based on the use of an exchange-correlation potential that depends *nonlocally* on the electron density at the surface and automatically yields the correct asymptotic shape of the surface Kohn-Sham potential. In our scheme the density-functional nonlocality originates in the insertion of long-range correlations into the electron self-energy, from which we evaluate the exchange-correlation potential for jellium. The solution to that problem is parametrized for use at real metal surfaces. Image-potential surface states and crystal-induced surface states are obtained on the same footing without any fitting parameters. We apply our method in calculations of the surface-electronic structure of (100) and (111) surfaces of aluminum and palladium. [S0163-1829(98)03423-7]

I. INTRODUCTION

There is a growing interest in accurate theoretical descriptions of the surface properties of solids. The reasons for this interest are manifold: First, experimental techniques have been developed that allow for detailed investigations of the surface, such as, e.g., two-photon-photoemission spectroscopy[1] (2PPE) and scanning-tunneling microscopy (STM).[2] A necessary condition for a full theoretical interpretation of the results of such experiments is an accurate description of the surface potential and the surface electronic structure.[3] Second, recent progress in the material sciences has led to the production of surfaces of high purity, and has allowed the design of various structures with desired properties. For the understanding of the physicochemical processes of these systems one needs a detailed knowledge of the electronic structure of these materials, and in this context surface states play an important role. Finally, the electronic-surface problem constitutes an interesting and demanding many-body system that attracts theoreticians *per se*.

On metal surfaces one observes two different types of surface states: crystal-induced and image-potential states. Crystal-induced surface states have maximal amplitude in the outermost crystal layers and decay rapidly into the bulk. They owe their existence to the modified boundary conditions for a Bloch state at the surface. In an infinitely extended crystal only Bloch states with real wave vector are allowed because otherwise the electron density becomes infinite. In a semi-infinite crystal solutions with complex wave vector $\vec{\kappa}$ can exist when the imaginary part of $\vec{\kappa}$ is perpendicular to the surface.[4] Image-potential states[5] have their origin in the particular shape of the surface barrier, which decays asymptotically as $1/z$, where z denotes the distance from the surface. As in the case of a hydrogen atom this potential can bind a Rydberg series of states just below the vacuum level. The binding energy of the first $(n=1)$ of these unoccupied states is typically 0.5–0.7 eV.

It is easy to understand the asymptotic form of the surface barrier classically. The method of image charges[6] yields $V(z)=-e^2/4z$ for a particle with charge e in front of a metal surface. However, this treatment does not address the microscopic many-body problem that is at the heart of a realistic quantum-mechanical calculation. In this case the image charge is identified with the exchange-correlation (XC) hole associated with an electron, in the limit that the electron is far out in the vacuum. Deep inside the crystal, the XC hole produced by each electron because of the Coulomb interaction and the Pauli principle is spherically symmetric (ignoring the crystal structure) and centered at the electron's position. When one removes an electron from the crystal—e.g., in an STM experiment—the electron and its XC hole first move towards the surface together. As the electron crosses the surface, the XC hole begins to distort from sphericity. When the electron has left the metal its XC hole has split from it, remaining at the metal surface.[7,8] This is a long-range correlation effect that yields a surface barrier that asymptotically has the form $V(z)=-e^2/4(z-z_0)$,[9] where z_0 denotes the effective image-plane position, which as a rule does not coincide with the geometrical surface.

The most successful theory in practical calculations for ''real'' many-electron systems is the density-functional theory of Hohenberg, Kohn, and Sham.[10] In the Kohn-Sham formulation the many-body problem is mapped onto a noninteracting-particle problem described by Schrödinger-like one-particle equation. All many-body effects are taken into account by an effective local potential, the XC potential, defined as the functional derivative of the XC energy functional E_{XC} with respect to the electron density $n(\vec{x})$,

$$V_{\mathrm{XC}}=\frac{\delta E_{\mathrm{XC}}[n(\vec{x})]}{\delta n(\vec{x})}. \tag{1}$$

In principle the Kohn-Sham method provides an exact description of the ground-state density and total energy of a many-electron system. Although there is no formal justification for interpreting the resulting one-electron-energy eigenvalues and wave functions as the corresponding quantities for real quasiparticles, such interpretation is often tacitly assumed—in many cases quite successfully. The key limitation in the application of the Kohn-Sham formalism is that one does not know the exact form of the XC energy functional. The simplest, and most widely used, approximation is the local density approximation (LDA).[11] In this approximation one assumes that the XC energy density is a local function of the density, i.e., one writes

$$E_{\mathrm{XC}}=\int d^3x n(\vec{x})\varepsilon_{\mathrm{XC}}[n(\vec{x}], \tag{2}$$

where $\varepsilon_{\mathrm{XC}}$ is the XC energy per electron for a *homogeneous* electron gas whose density is equal to local $n(\vec{x})$. This approximation gives total energies, lattice constants, bulk moduli, etc. usually in good agreement with experiment.[11] However, because of the neglect of long-range electron correlations described above, and in the presence of the strong inhomogeneity of the electron density at a surface, the LDA yields a *qualitatively incorrect* surface barrier: instead of decaying like $1/z$ the LDA XC potential decays exponentially. It is therefore not possible to describe image-potential states—and other important phenomena associated with long-range correlations, such as Van der Waals forces—within the framework of the LDA.

Previous calculations of image states introduced the correct asymptotics ''by hand'' and used the position of the image plane as a fitting parameter to reproduce experimental findings.[12] An exception was the calculation of Ossicini, Bertoni, and Gies,[13] who obtained a Kohn-Sham potential with an imagelike tail through the use of an ansatz for the exchange correlation functional introduced by Gunnarsson and Jones.[14] However, such ad hoc procedure leads to unphysical results for the XC hole at the surface. By contrast to these previous attempts, we use in this work an XC potential that was derived from the interrelation between many-body perturbation theory and density-functional theory. Such procedure treated the long-range correlations and abrupt density variation at the surface properly, and thus the surface barrier shows the correct asymptotic behavior.[15,16]

The main purpose of this paper is to utilize the nonlocal framework of Eguiluz *et al.*[15,16] and to report *ab initio* calculations for real metals, in which the crystal induced and the image-potential states are treated on the same footing without the use of any fitting parameters, and result automatically. We illustrate the method by applying it to the case of (100) and (111) surfaces of the simple metal aluminum and of the transition-metal palladium.

In Sec. II A we describe how the nonlocal XC potential is obtained. In Sec. II B we show how the nonlocal potential can be used in realistic band-structure calculations. In Secs. III and IV we present our results for aluminum and palladium, which we compare with available experimental and theoretical results. The last section consists of a summary and outlook.

II. THE METHOD

A. Construction of a nonlocal exchange-correlation potential

The limitations of the LDA in describing correctly the surface barrier of a crystal is due to the neglect of long-range correlations and the fact that the strong charge inhomogeneity that occurs at a surface is not properly accounted for. In order to improve over LDA description of the surface barrier one has to take into account inhomogeneity from the outset and thereby retain the nonlocality of the XC energy functional. Therefore, the XC potential that we use in this work is not derived for a homogeneous electron gas but for a jellium surface. The starting point is an exact integral equation that relates the local, energy-independent XC potential of density-functional theory, V_{XC}, with the nonlocal, energy-dependent self-energy of many-body theory, Σ_{XC}, namely,

$$\int d^3x_1 V_{\mathrm{XC}}(\vec{x}_1)\int dE g_0(\vec{x},\vec{x}_1;E)g(\vec{x}_1,\vec{x};E)$$
$$=\int d^3x_1\int d^3x_2\int dE g_0(\vec{x},\vec{x}_1;E)\Sigma_{\mathrm{XC}}$$
$$\times(\vec{x}_1,\vec{x}_2;E)g(\vec{x}_2,\vec{x};E). \tag{3}$$

The Green's function g entering Eq. (1) describes the propagation of a real quasiparticle, while g_0 describes the propagation of a Kohn-Sham electron. This integral equation was derived by Sham and Schlüter,[17] and used by Godby *et al.*[18] and also by Hanke and Sham[19] for the investigation of the band gap in semiconductors and insulators. For technical details of the solution of this equation for a jellium surface the reader is referred to Refs. 15 and 16. In that work the self-energy is evaluated in the *GW* approximation,[20] i.e., written as the convolution of the propagator g and the dynamically screened Coulomb interaction W,

$$\Sigma_{\mathrm{XC}}(\vec{x}_1,\vec{x}_2;E)=\frac{i}{2\pi}\int dE' e^{iE'\eta}g(\vec{x}_1,\vec{x}_2;E+E')$$
$$\times W(\vec{x}_1,\vec{x}_2;E'). \tag{4}$$

The screened Coulomb interaction W is given in terms of the bare Coulomb interaction v and the density-density response function χ_T,

$$W=v+v\chi_T v, \tag{5}$$

where $\chi_T=\tilde{\chi}+\tilde{\chi}v\chi_T$. The irreducible polarizability $\tilde{\chi}$ is calculated in RPA, which from the diagrammatic point of view is completely consistent with Eq. (4).[21] As is commonly assumed in *ab initio* applications of the *GW* approximation, the substitution of the Kohn-Sham propagator g_0 for the many-body propagator g in Eq. (4) is a good approximation. This assumption, which we follow also in this work, stems from computer CPU limitations for iterating Eq. (4) to self-consistency ''in g.'' We iterate, however, the Kohn-Sham equations with V_{XC} given by Eq. (3) in order to built in the long-range correlations into the Kohn-Sham propagator g_0. Thus, from the viewpoint of the inclusion of long-range correlations, is our method fully self-consistent.

The solution of the integral equation, Eq. (3), with the self-energy Σ_{XC} provided by Eqs. (4) and (5) yields an XC

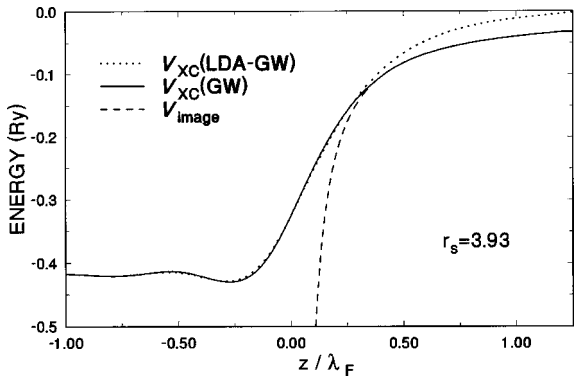

FIG. 1. Exchange-correlation potential for the jellium surface with bulk density of sodium, $r_S=3.93$ ($\lambda_F=12.9$ a.u.). The solid line shows the solution of Eq. (1) within the *GW* approximation for $\Sigma_{\rm XC}$, the dotted curve shows the corresponding LDA potential, and the dashed curve is a pure image potential $V_{\rm im}(z)=-e^2/4(z-z_0)$.

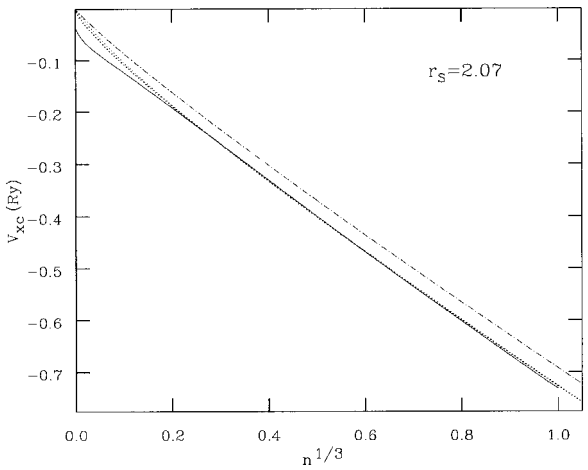

FIG. 2. The *GW*-based ''nonlocal'' exchange-correlation potential (solid line) as a function of $n^{1/3}$. Also plotted are the *GW*-LDA potential (dotted line) and the Ceperley-Alder LDA potential (dashed-dotted line). Except for very small densities the *GW*-LDA potential is identical to the XC potential of von Barth and Hedin, Ref. 24 (another dotted line).

potential with the correct asymptotic form far from the surface.[16] The solid line in Fig. 1 shows such a solution for a metal whose density is in the middle of the range of metallic densities. The $-e^2/4z$ image limit of the surface barrier is due to the Coulomb correlations originated by the second term on the right-hand side (rhs) of Eq. (5). The exchange-only potential, i.e., due to the bare Coulomb interaction [first term on the rhs of Eq. (5)], tends to $-a/z^2$ for large z, thus contributing to the position of the image plane.[16] Now, one can define an *GW*-LDA exchange-correlation potential, $V_{\rm XC}^{\rm LDA}$, within the framework of Eqs. (3)–(5) as the solution of the integral equation for the homogeneous case. Such a solution is simply given by $V_{\rm XC}^{\rm LDA}=\Sigma_{\rm XC}(k=k_F;E=E_F)$. The $V_{\rm XC}^{\rm LDA}$ potential is shown as the dotted line on Fig. 1. The $V_{\rm XC}^{\rm LDA}$ yields, however, an incorrect asymptotic decay. This means that for distances from the surface on the order of λ_F (the Fermi wavelength), which is relevant for STM experiments, the LDA potential differs from the correct image potential by nearly 1 eV. On the other hand, it is important to note that in the bulk and close to the surface the nonlocal potential and the LDA potential are basically indistinguishable.

B. Realistic band-structure calculations in the presence of long-range correlations

In the previous section an approach was outlined to derive a density-functional potential at a surface of a solid, which although is a local potential in space, depends nonlocally on the electron density and shows a correct asymptotic behavior in vacuum. The approach is general and in principle applies to any system, however, the self-consistent solution of Eqs. (3)–(5) is at present computationally extremely difficult at the surface of a real solid. Therefore, in previous papers[16] a new method of the construction of the Kohn-Sham potential at a metal surface was proposed beyond the usual local-density approximation. The idea is very simple: instead of assuming locally (i.e., in small portions of space) the exchange-correlation potential of the *homogeneous electron gas*, determined by the value of the local electron density n, we take outside the metal surface the *nonlocal* exchange-correlation potential of the jellium surface calculated from Eqs. (3)–(5). For this reason we parametrize the functional dependence of the jellium-surface nonlocal potential $V_{\rm XC}(r_S,z)$ on the electron density $n(z)$, with which it is self-consistent. Such a parametrization is possible because from the first Friedel peak out into the vacuum there exists a one-to-one correspondence between both sets of values. As is the case in the LDA approximation, the electron density must be self-consistently determined through the iterational procedure. The resulting surface potential of a metal shows the image tail, because the long-range Coulomb correlations responsible for this tail are built into the XC potential used.

In our calculations we use a parametrization of the functional dependence of $V_{\rm XC}$ on n by a set of spline coefficients for the vacuum region. Inside the crystal we use the XC potential obtained in the *GW*-LDA. This potential is shown in Fig. 1 by the dotted line. Both potentials are identical deep inside the metal and turn out to be indistinquishable even at the jellium edge, therefore such a procedure is fully justified and is only a convenient way of including surface nonlocal effects in practical calculations in which many (also infinitely many) crystal layers are used. Where the two potentials deviate is the region of small densities out of the metal surface. In particular, it is seen in Fig. 2 that all the LDA potentials approach zero faster than the ''nonlocal'' potential. In the way the ''nonlocal'' potential approaches zero is implicitly included in its image shape. Since the nonlocal potential $V_{\rm XC}$ is parametrized, its use in the band-structure codes for real systems is as easy as is the use of the conventional local-density approximation. An iterative solution of the Kohn-Sham equation in the presence of the nonlocal $V_{\rm XC}$ yields a self-consistent potential, in which both long-range correlations and crystal effects are included in the same time.

The dashed-dotted curve in Fig. 2 shows the Ceperley-Alder XC potential.[22] It is in the whole range of densities a few tenths of an eV higher than the new potential.[23] Therefore, the work function we get with the new potential is always higher than that obtained with the Ceperley-Alder potential. The reason for this difference is not a specific surface problem. It comes from the fact that the RPA correlation

energy (therefore also V_{XC}) for the homogeneous electron gas differs from the quantum Monte Carlo results by about 10%. In principle this difference should be ''absorbed'' by the self-consistent inclusion of vertex correction.[20] There are some indications that the simple form of the vertex provided by the time-dependent LDA theory could be useful here.[25]

One of the consequences of the nonlocality of the new XC potential is that it not only depends on the local density n but also on the bulk density r_S of the jellium. Thus, a question is posed at the outset: what is the proper choice of r_S for a given metal? This is a long-standing question and several prescriptions exist for the choice of a proper r_S for a metal. While for simple metals the choice based on the average charge density works very well, for d metals the situation is more complicated and it is not *a priori* obvious what prescription is appropriate. Our choice is the following: We first calculate within LDA the charge density and self-consistent potential for the bulk of this metal. From this calculation we deduce an effective r_S by averaging the XC potential over a bulk unit cell. In other words, we solve for r_S the following equation: $V_{XC}(r_S)=\overline{V_{XC}}$, where the jellium $V_{XC}(r_S)$ and the unit-cell average $\overline{V_{XC}}$ of a real crystal must be calculated within the same LDA scheme. Independently of the LDA scheme used (i.e., Ceperley-Alder or *GW*-LDA), this procedure yields for aluminum $r_S=2.07$, the value that is commonly found in the literature. For palladium we determine $r_S=1.50$. Interestingly, this value is very close to the value $r_S=1.51$, which one needs to reproduce the main experimental plasmon peak of palladium with a simple, free-electron formula.[26]

C. Technical details

We performed density-functional calculations in the periodic slab geometry using norm-conserving pseudopotentials of the Bachelet-Hamann-Schlüter type.[27] Our basis consisted of plane waves for aluminum and additionally 5 d-type Gaussians at each atomic site for palladium. The energy cutoff for plane waves was 9.5 Ry for Al and 12.5 Ry for Pd. Integrations in $\vec{k}$ space were performed with a uniform mesh of Monkhorst and Pack points[28] and a Gaussian energy smearing scheme for the determination of the Fermi level.[29] As an artifact of the slab geometry all surface states occur pairwise, one from each surface of the slab. For an infinitely thick slab the two states would be degenerate but for finite slabs the two states hybridize and the degeneracy is lifted. The splitting depends on the thickness of the film (for *usual* surface states), the width of the vacuum region (for *image* surface states) and the decay properties of a given state. Since on surfaces of both aluminum and palladium there are surface states decaying slowly, in order to determine unambiguously the energy position of surface states one should use very big slabs. We have performed therefore our calculation in two steps: First, we determine the self-consistent surface potential with smaller slabs, typically 7 or 9 crystal layers and 6 to 9 vacuum layers. Such constructed slabs proved big enough to calculate accurate self-consistent surface potential, but were too thin from the point of view of the hybridization just alluded to. Thus, in the next step, for the calculations of the surface-electronic structure we widened our slabs by inserting an appropriate number (16–39) of ''bulk'' layers, for which the potential equals the self-consistent potential of the central layers in our original thin slab. The rationale for this stretching procedure is that the potential so defined should be very close to the self-consistent potential for the stretched slab, which one would get from a costly iterational procedure. Finally, since the image states tail far out into the vacuum, it was necessary to stretch also the vacuum, for aluminum as well as for palladium. We first determined the image-plane position from the self-consistent potential of the thin slab and used this to extrapolate the potential sufficiently far out into the vacuum.

TABLE I. Image-plane positions for different aluminum surfaces and jellium of $r_S=2.07$. Values are given in atomic units with respect to the jellium edge. In first three rows the image-plane position is obtained from the tail of V_{XC}; in the last row, from the centroid of the induced charge.

Al(001)	Tail of V_{XC}	0.54
Al(111)	Tail of V_{XC}	0.38
Jellium	Tail of V_{XC}	0.72
Jellium	Linear response	1.49

III. RESULTS FOR Al(100) AND Al(111)

In order to study the electronic structure of aluminum surfaces we first calculated the self-consistent, *nonlocal* Kohn-Sham potential for a periodically repeated supercell that consisted of 9 crystal layers and 7 or 6 vacuum layers for the (100) or (111) surface, respectively. The corresponding work function is 4.59 eV for Al(100) and 4.82 eV for Al(111). These values are about 0.4 eV higher than those obtained with the Ceperley-Alder LDA formula for exchange and correlation.[30] This difference (illustrated in Fig. 2) is due to the overestimate of the correlation energy of the homogeneous electron gas by the RPA (or GW) self-energy diagram.[18] On the other hand, the values of work function determined with the Ceperley-Alder potential[30] are in very good agreement with experiment.[31]

From an analysis of the long-range (long distance) form of the self-consistent potential we can determine the image-plane positions z_0. The values, calculated for Al(100), Al(111) and for jellium with $r_S=2.07$, are listed in Table I. The first three numbers were obtained via a χ^2 fit from the planar average of the XC potential in the vacuum. The last row gives the value one obtains in the linear response theory,[32] in which the image-plane position is identified with the center of mass of the charge induced by an external classical test charge placed infinitely far away from the surface. An immediate conclusion drawn from Table I is that the image-plane position derived from the image tail of V_{XC} is much closer to the surface than its counterpart determined within linear response. This is because in the case of an external classical charge there are no exchange processes that contribute to building up the surface barrier.[16] Therefore the image plane position is different for *a Kohn-Sham electron of the quantum system* and for an external test charge. Our value for z_0 for jellium of $r_S=2.07$ is 0.72. It is substantially smaller than our result from the linear response theory ($z_0=1.49$), or the analogous result of Lang and Kohn ($z_0=1.60$).[32] Our result is consistent with the result of Ossicini,

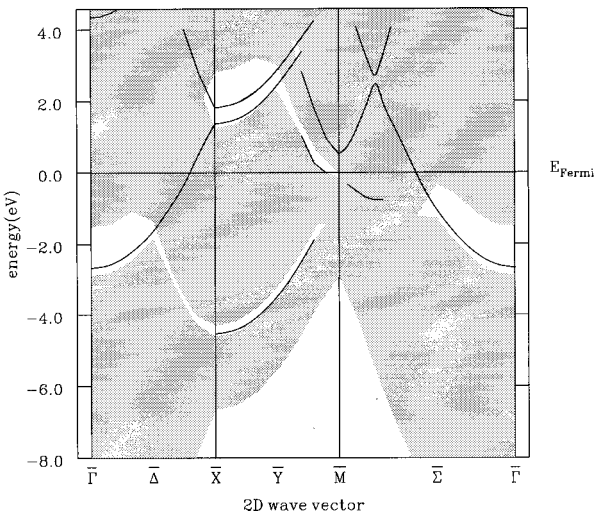

FIG. 3. Projected bulk band structure and electronic surface states for energies below the vacuum level for Al(100). The free-electron-like band close to the vacuum level around $\bar{\Gamma}$ corresponds to the image-state resonances.

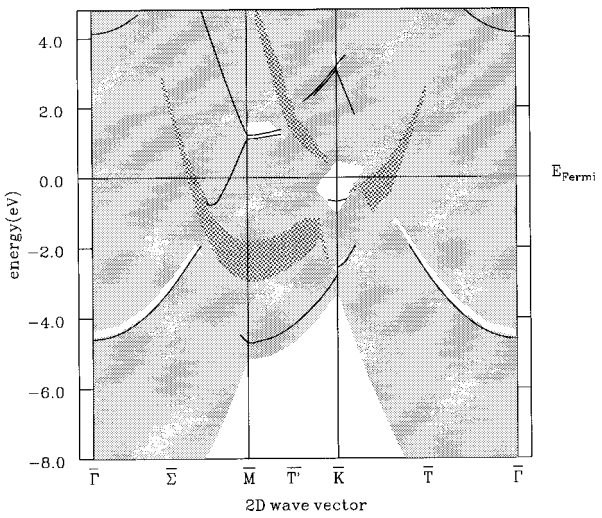

FIG. 4. Projected bulk band-structure and electronic surface states for energies below the vacuum level for Al(111). The free-electron-like band close to the vacuum level around $\bar{\Gamma}$ corresponds to the image-state resonances. The dark-shadowed areas correspond to broad surface resonances. For a full discussion of these states see Ref. 30.

Bertoni, and Gies,[13] who have obtained the value of $z_0 = 0.85$ for the surface of jellium of $r_S = 2.0$ from the Kohn-Sham potential calculated within a model ansatz for the exchange correlation functional of Gunnarsson and Jones.[14]

One can also conclude from Table I that the inclusion of the ion cores brings a further significant decrease of the position of z_0. This fact was also shown by Inglesfield,[33] who obtained a value of $z_0 = 1.1$ for a realistic model of Al(100). He identified the image-plane position with the center of gravity of the induced charge under the influence of an external electric field; therefore, his z_0 is relevant for an external classical charge.

The surface states for the (100) and the (111) face of aluminum are shown in Figs. 3 and 4, respectively. They were calculated after stretching either the metal or the vacuum part of the slab by inserting up to 39 crystal, or vacuum layers. The shadowed area in these figures shows the projected bulk band structure. Solid lines correspond to surface states or surface resonances. The dark shadowed areas in Fig. 4 indicate broad surface resonances.[30] The free-electron-like band close to the vacuum level around $\bar{\Gamma}$ corresponds to image states. The energy positions of the crystal-induced surface states, measured with respect to the Fermi level, agree to within a few hundreths of an electronvolt with the results of our LDA calculation where we used the Ceperley-Alder XC potential. The results of this LDA calculation are described in detail elsewhere.[30]

Yang, Bartynski, and Vanderbilt investigated recently the unoccupied electronic structure of Al(111) via the k-resolved inverse-photoemission spectroscopy.[34] Due to the experimental setup not the whole energy-momentum space was probed in these measurements and some data are reported in the higher energy region than considered in the present calculation. In addition, it is difficult to distinguish fully unambiguously in experiment between the bulk and surface structures. Nevertheless, the remarkable observation is in very good agreement with experiment, both in position and dispersion, for the unoccupied ''broad'' resonance in the middle of the $\bar{\Gamma}\,\bar{M}$ line (see Fig. 3 of Ref. 34).

Yang *et al.*[34,35] and previousely Heskett *et al.*[36] have reported in their inverse photoemission experiments an image-state resonance at the Al(111) surface located 0.45 eV below the vacuum level. As seen in Figs. 3 and 4, on the (100) as well as on the (111) surface we obtain an $n=1$ image state with the binding energy of about 0.4 eV, which agrees rather well with experiment. Because on both surfaces there is no gap in the projected bulk band structure around the $\bar{\Gamma}$ point in the relevant energy range, these image states are resonances. In our slab calculation we find a number of eigenstates with $n=1$ character that occur over a finite range of energy. Due to the finite thickness of the slab the splitting between these states is fairly large and it is difficult to determine the energy location of the $n=1$ member of the Rydberg series. It turned out that with the present periodic-slab technique, very big slabs must be used, in order to resolve computationally for the $n=1$ image state. However, because of the small corrugation of the potential inside the vacuum region and the vanishing amplitude of image states inside the bulk of the metal, the energy of the image states could be determined from an additional calculation using a one-dimensional model. In this model the planar average of the self-consistent potential of the three-dimensional slab was taken in the Hamilton operator. Such a one-dimensional model allows for much bigger slabs of several hundred layers and therefore for better computational resolution in the calculation of the density of states that we use to determine the energy position of surface resonances.

IV. RESULTS FOR Pd(100) AND Pd(111)

As noted above, in our calculations for the transition-metal palladium our basis consisted of plane waves plus five d-type Gaussians at each atomic site. As in the case of alu-

minum, we have determined in a first step the self-consistent surface potential for thin slabs; in the present case the number of metal layers was set to seven. Then, in the investigation of the *usual* crystal-terminated surface states we stretched the slab in its bulk region to include 19 metal layers, while in the investigation of *image* states the vacuum portion of the slab was stretched to include 19 (empty) layers. This proved enough to observe the $n=1$ image state, which on both surfaces is a *sharp* state within the gap in the projected bulk band structure. We therefore need not to evoke the one-dimentional potential model in the study of image states of Pd.

The work function obtained with the nonlocal potential V_{XC} is 6.11 and 6.18 eV for Pd(100) and Pd(111), respectively. For reasons discussed above, these numbers are larger than those resulting from the Ceperley-Alder exchange-correlation potential, which are 5.68 and 5.75 eV for Pd(100) and Pd(111), respectively. Both sets of numbers differ somewhat from experiment. The experimental value of the work function for Pd(100) is 5.8 eV,[37] while for Pd(111) two investigations, both via the two-photon photoemission (2PPE) technique, give different values: Kubiak[38] reports a work function of 5.55 eV, Fischer *et al.*[39] obtain a work function of 5.44 eV. Our disagreement with experiment, especially for Pd(111), is a bit surprising. It could be caused either by purely technical reasons, or the reason could be of a more fundamental nature, indicating limitations of our method. In regard to the technical reasons, it is possible that doing a calculation of a better technical quality (which is ''in principle'' always possible), i.e., allowing for larger slabs or extending the variational freedom by solving Kohn-Sham equation at the surface, could help to some extent. More probable technical reason is, however, a proper choice of a corresponding jellium for which the nonlocal surface potential is calculated and used in a ''real metal'' calculation. In regard to more fundamental reasons, let us note that a part of the difference between our theoretical value of the work function and the experimental value could be ''absorbed'' by a proper choice of a vertex function to the self-energy of jellium.[20] Most probably, this is the difference between both our theoretical values: the one obtained with the nonlocal potential and the one resulting from the Ceperley-Alder potential. What remains could be due to either technical reasons or the inapplicability of the jellium-derived nonlocal potential V_{XC} to the case of a transition metal surface. This question demands further studies.

A. Pd(100)

Our results for the surface states of the (100) face are compiled in Fig. 5. Overall they agree very well with the calculation of Gay *et al.*;[40] however, due to the less stringent criterion for selection of surface states we adopt, our surface electronic structure is more far reaching. In particular, we include among surface resonances groups of states that in a certain energy region have a pronounced surface amplitude, but otherwise propagate periodically like normal bulk states into the volume of the crystal. Such ''broad surface resonances'' predicted by us for Al(111) according to the same criterion,[30] have been later on reported experimentally.[34] The occupied states have been investigated by Elliot *et al.*[41] by means of angle-resolved photoemission spectroscopy. While

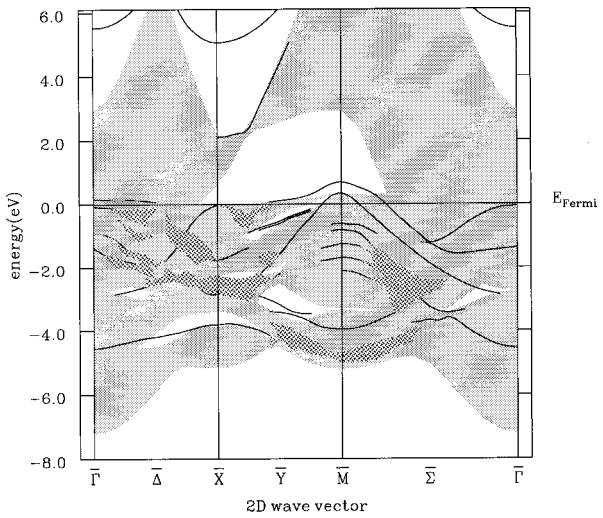

FIG. 5. Projected bulk band structure and electronic surface states for Pd(100). Free-electron bands in the gaps around the $\bar{\Gamma}$ point, just below the vacuum level, correspond to the $n=1$ image state. The dark shadowed areas are the regions of ''broad resonances'' described in the text.

we find that there is a qualitative agreement between our results and these experimental data, a question remains as to why so few states were detected experimentally compared with the number predicted theoretically. In addition, the dispersion of the lower experimental state from $\bar{\Gamma}$ to $\bar{X}$ is somewhat different from our picture, but here the problem of the connectivity of bands derived within a finite slab can play a role. Finally, experimental data of Elliot *et al.* show fairly broad features, which the authors interpret as being due to many-body effects. Such an interpretation need not be necessarily correct and the broad experimental features can hide fine structures.

Wu *et al.*[37] observed an unoccupied surface resonance at $\bar{\Gamma}$, 1.0 ± 0.2 eV above the Fermi level, in their inverse photoemission experiments on the Pd(100) surface. In our calculation we do not find any resonance in this energy range, neither was it found in the LDA calculation by Gay *et al.*[40] An unoccupied resonance at $\bar{\Gamma}$ was predicted in a calculation by Smith *et al.*,[42] it was placed, however, at somewhat higher energy (1.5–2.0 eV) and the calculation was based on a simplified, one-dimensional model of the surface potential. Experimentally the resolution of the low-lying unoccupied surface resonances is very difficult, because they overlap with a strong bulk peak due to the transitions into *d* bands. Since the accuracy of the inverse-photoemission technique is generally not too high, we think that the unoccupied surface electronic structure of Pd(100) needs still an independent experimental determination with high-precision means.

A similar situation occurs at the $\bar{X}$ point. Here Wu *et al.*[37] have observed a resonance at 1.0 ± 0.2 eV above the Fermi level, which was previously predicted in model calculations of Smith *et al.*,[42] but which we do not find in our calculation. We find a resonance that starts at 2.1 eV at the $\bar{X}$ point and follows up along the very edge of the energy gap in $\bar{X}\,\bar{M}$ direction. This state was also predicted by Gay *et al.*[40] In the

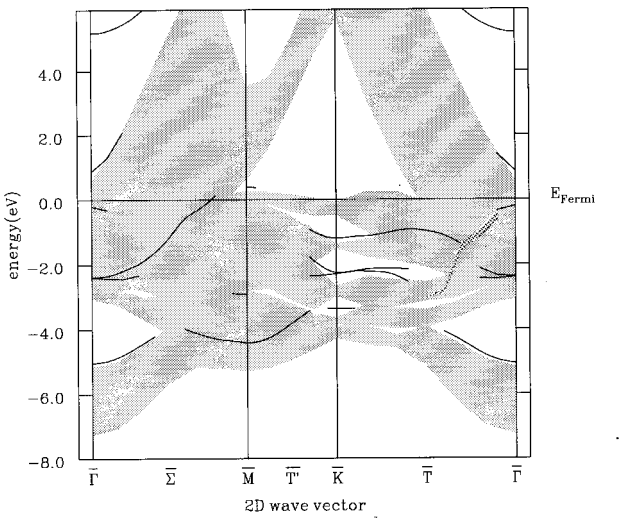

FIG. 6. Projected bulk band structure and electronic surface states for Pd(111). See caption to Fig. 5.

same gap around the $\bar{X}$ point we find another very sharp unoccupied surface band at 5.1 eV, which was so far not detected experimentally. At the $\bar{M}$ point Wu *et al.*[37] detected two surface states in the gap, one at 0.8 ± 0.2 eV and another at 2.5 ± 0.2 eV above the Fermi level. The energy location of the lower state agrees well with the energy of the state we find at 0.74 eV above E_F.

Now we come to discuss the image states. They are shown in Fig. 5 as free-electron parabola below the vacuum level close to the $\bar{\Gamma}$ point. From an analysis of the image tail of $V_{\rm XC}$, we determine the image plane to be at 0.47 a.u. outside the geometrical surface. This agrees quite well with the value $z_0=0.55$ a.u., which was obtained in a model calculation by Smith *et al.*,[42] in which an empirical, one-dimensional barrier was fitted to the planar average of an LDA slab calculation.

We find the $n=1$ image state at $\bar{\Gamma}$ at 0.60 eV below the vacuum level; it has a free electronlike dispersion with an effective mass $m^*=1.04m_e$. This result agrees well with the value predicted by Smith *et al.*[42] ($E_{n=1}=-0.53$ eV). On the other hand, Wu *et al.*[37] report an experimental value of 0.9 ± 0.2 eV for the $n=1$ image state. This value seems, however, unusually large.

Summarizing, the comparison with experiment for the (100) face of Pd seems somewhat unsettled. There are a few experimentally obtained surface structures that are not present in our results, while we predict some states that were not seen in experiment. There is still a possibility that inclusion of many-body effects associated with the presence of the *d* bands could improve the agreement with available measurements. We believe, however, that before such a hypothesis is advanced, it would be extremely useful to extend the existing experimental database with results obtained with high-resolution methods.

B. Pd(111)

We present our results for the surface states of Pd(111) in Fig. 6. For the crystal induced states we have basically the same results as Louie,[43] who also performed a mixed-basis pseudopotential calculation. A slight shift in the relative position of calculated states with respect to the Fermi level between our results could originate from the quality of pseudopotentials used in both calculations. We use in this work an *ab initio* norm-conserving scalar-relativistic pseudopotential, not available yet in the time the calculation of Louie was performed.

As we already noted, the experimental investigation of the occupied crystal-induced surface states is difficult because there are many bulk transitions from *d* bands in the photoemission spectra. To our knowledge the most recent experiment has been performed by Eberhardt *et al.*,[44] who found two occupied states at $\bar{\Gamma}$, one at 0.3 eV below E_F, and another one at 2.2 eV below E_F. These energies agree well with our results, which are -0.2 and -2.45 eV, respectively. At $\bar{K}$ Eberhardt *et al.* detected states at 0.3 eV and at 2.1 eV below the Fermi level. In this case only the energy of the lower state agrees well with our result, which is -2.25 eV; we find the higher state at 1.2 eV below E_F. At the $\bar{M}$ point neither our calculation nor that of Louie[43] yielded a state detected experimentally[44] at about 1 eV below E_F.

The unoccupied surface states have been investigated by Hulbert *et al.* via the inverse photoemission technique.[45] They found a surface state at $\bar{\Gamma}$ with an energy of 1.3 eV and a free-electron-like dispersion of an effective mass $m^*=0.3m_e$. In our calculation we predict an unoccupied surface state with the energy of 0.9 eV and the effective mass $m^*=0.22m_e$.

Our value of the image-plane position is $z_0=0.35$ a.u. outside the nominal jellium edge (geometrical surface). The energy of the $n=1$ image state is in our calculation -0.69 eV with respect to the vacuum level, and its effective mass is $1.03m_e$. There is considerable scatter in the experimental results for the binding energy of this state. The inverse photoemission experiment of Hulbert *et al.*[45] gave a binding energy of 0.5 eV. The effective mass was reported to be 1.0, in accordance with all other experiments. Conrad *et al.*[46] measured the elastic electron reflectivity at the zone boundary. By extrapolating their results to the zone center they determined a binding energy of 0.75 eV. In the 2PPE measurement, Kubiak[38] found the image state at 0.65 ± 0.1 eV below the vacuum level. Finally, the most recent and probably most accurate 2PPE experiment of Fischer *et al.*[39] yielded a binding energy of 0.55 eV.

V. SUMMARY

We have presented density-functional calculations to determine the electronic structure of low index surfaces of aluminum and palladium. In the evaluation of the electronic structure we use an XC potential in which long-range correlations are taken into account. Therefore, the calculated surface barrier automatically includes the correct asymptotic behavior, namely, the $1/z$ decay, which is responsible for the existence of the image-potential surface states. We are therefore able to calculate crystal-induced and image-potential states on the same footing, without any fitting parameters. For sp-bonded Al the agreement of our results with experiment is very good. For transition-metal Pd the agreement is

less satisfactory, especially for the (100) face; however, in this case too few experimental data exist to allow for definitive conclusions. It is also possible that this disagreement is the result of our tacitly assumed equivalence between Kohn-Sham eigenvalues and real excitation energies. However, recent many-body calculations for a jellium surface show that the energy position and shape of the wave function of image states are very well represented by the Kohn-Sham states, once the nonlocality of the XC energy is taken into account in the XC potential.[47] Whether the same is true for a transition metal such as palladium is still an open question.

ACKNOWLEDGMENTS

We acknowledge support from the BMFT Contract No. 03-HA2WUE (M.H. and W.H.), from the DFG Grant No. HA 1537/1-8 (A.F. and W.H.), and from the NSF Grant No. DMR-9207747 (A.G.E.). A.G.E. also acknowledges support from the San Diego Supercomputer Center, and from the National Energy Research Supercomputer Center. The Solid State Division, Oak Ridge National Laboratory is managed by Lockheed Martin Energy Systems, Inc., for the Division of Materials Sciences, U.S. DOE under Contract No. DE-AC05-84OR21400.

[1] R. W. Schoenlein, J. G. Fujimoto, G. L. Eesley, and T. W. Capehart, Phys. Rev. Lett. **61**, 2596 (1988); Phys. Rev. B **41**, 5436 (1990); W. Steinman, Appl. Phys. A: Solids Surf. **49**, 365 (1989).

[2] G. Binnig, N. Garcia, H. Rohrer, J. M. Soler, and F. Flores, Phys. Rev. B **30**, 4816 (1984); B. N. J. Persson and A. Baratoff, *ibid.* **38**, 9616 (1988); A. A. Lucas, H. Morawitz, G. R. Henry, J.-P. Vigneron, Ph. Lambin, P. H. Cutler, and T. E. Feuchtwang, *ibid.* **37**, 10 708 (1988); P. M. Echenique, A. Grass-Marti, J. R. Manson, and R. H. Ritchie, *ibid.* **35**, 7357 (1987).

[3] G. Doyen, E. Koetler, J.-P. Vigneron, and M. Scheffler, Appl. Phys. A: Solids Surf. **51**, 281 (1990).

[4] N. W. Ashcroft and N. D. Mermin, *Solid State Physics* (Sounders College Publishing, Fort Worth, 1976).

[5] P. M. Echenique and J. B. Pendry, J. Phys. C **11**, 2065 (1978); N. V. Smith, Phys. Rev. B **32**, 3549 (1985).

[6] J. D. Jackson, *Classical Electrodynamics* (Wiley, New York, 1962).

[7] X.-P. Li, R. J. Needs, R. M. Martin, and D. M. Ceperley, Phys. Rev. B **45**, 6124 (1992).

[8] J. M. Pitarke and A. G. Eguiluz (unpublished).

[9] L. J. Sham, Phys. Rev. B **32**, 3876 (1985); N. D. Lang, in *Theory of the Inhomogeneous Electron Gas*, edited by S. Lundqvist and N. H. March (Plenum, New York, 1983); J. E. Inglesfield and I. D. Moore, Solid State Commun. **26**, 867 (1978); J. C. Inkson, J. Phys. C **10**, 567 (1977); J. Bardeen, Surf. Sci. **2**, 381 (1964).

[10] P. Hohenberg and W. Kohn, Phys. Rev. **136**, B864 (1964); W. Kohn and L. J. Sham, Phys. Rev. **140**, A1133 (1965).

[11] For recent developments in density functional theory see, e.g., *Density Functional Theory of Many-Fermion Systems*, edited by S. B. Trickey (Academic, New York, 1990); and R. M. Dreizler and E. K. U. Gross, *Density Functional Theory: An Approach to the Quantum Many-Body Problem* (Springer, Berlin, 1990).

[12] For a review of calculations of image states see, for example, P. M. Echenique and M. E. Uranga, Surf. Sci. **247**, 125 (1991).

[13] S. Ossicini, C. M. Bertoni, and P. Gies, Europhys. Lett. **1**, 661 (1986); Surf. Sci. **178**, 244 (1986).

[14] O. Gunnarsson and R. O. Jones, Phys. Scr. **21**, 394 (1980).

[15] A. G. Eguiluz and W. Hanke, Phys. Rev. B **39**, 10 433 (1989).

[16] A. G. Eguiluz, M. Heinrichsmeier, A. Fleszar, and W. Hanke, Phys. Rev. Lett. **68**, 1359 (1992); A. G. Eguiluz, J. J. Deisz, M. Heinrichsmeier, A. Fleszar, and W. Hanke, Int. J. Quantum Chem., Symp. **26**, 837 (1992).

[17] L. J. Sham and M. Schlüter, Phys. Rev. Lett. **51**, 1888 (1983).

[18] R. W. Godby, M. Schlüter, and L. J. Sham, Phys. Rev. Lett. **56**, 2415 (1986); Phys. Rev. B **37**, 10 159 (1988).

[19] W. Hanke and L. J. Sham, Phys. Rev. B **13**, 361 (1988).

[20] L. Hedin and S. Lundqvist, in *Solid State Physics*, edited by H. Ehrenreich, F. Seitz, and D. Turnbull (Academic, New York, 1969), Vol. 23, p. 1.

[21] G. Mahan, Comments Condens. Matter Phys. **16**, 333 (1994).

[22] D. M. Ceperley and B. I. Alder, Phys. Rev. Lett. **45**, 566 (1980). In this work we use the parametrization of Ceperley-Alder results due to P. Perdew and A. Zunger, Phys. Rev. B **23**, 5048 (1981).

[23] This fact was also observed by Godby, Schlüter, and Sham (Ref. 18).

[24] U. von Barth and L. Hedin, J. Phys. C **5**, 1629 (1972).

[25] R. Del Sole, Lucia Reining, and R. W. Godby, Phys. Rev. B **49**, 8024 (1994).

[26] D. Isaacson, report.

[27] G. B. Bachelet, D. R. Hamann, and M. Schlüter, Phys. Rev. B **26**, 4199 (1982).

[28] H. J. Monkhorst and J. D. Pack, Phys. Rev. B **13**, 5188 (1976).

[29] C. L. Fu and K. M. Ho, Phys. Rev. B **28**, 5480 (1983); K. M. Ho, C. L. Fu, and B. N. Harmon, Phys. Rev. B **29**, 1575 (1984).

[30] M. Heinrichsmeier, A. Fleszar, and A. G. Eguiluz, Surf. Sci. **285**, 129 (1993).

[31] J. K. Grepstad, P. O. Gartland, and B. J. Slagsvold, Surf. Sci. **57**, 348 (1976).

[32] N. D. Lang and W. Kohn, Phys. Rev. B **7**, 354 (1973).

[33] J. E. Inglesfield, Surf. Sci. **188**, L701 (1987).

[34] S. Yang, R. A. Bartynski, and D. Vanderbilt, Phys. Rev. B **50**, 12 025 (1994).

[35] S. Yang, R. A. Bartynski, G. P. Kochanski, S. Papadia, T. Fondén, and M. Persson, Phys. Rev. Lett. **70**, 849 (1993).

[36] D. Heskett, K.-H. Frank, K. Horn, E. Koch, H. J. Freund, A. Baddorf, K. D. Tseui, and E. W. Plummer, Phys. Rev. B **37**, 10 387 (1988).

[37] S. C. Wu, D. M. Poirier, M. B. Jost, and J. H. Weaver, Phys. Rev. B **45**, 8709 (1992).

[38] G. D. Kubiak, J. Vac. Sci. Technol. A **5**, 731 (1987).

[39] R. Fischer, S. Schuppler, N. Fischer, Th. Fauster, and W. Steinmann, Phys. Rev. Lett. **70**, 654 (1993); S. Schuppler, N. Fischer, Th. Fauster, and W. Steinmann, Phys. Rev. B **46**, 13 539 (1992).

[40] J. G. Gay, J. R. Smith, F. J. Arlinghaus, and T. W. Capehart, Phys. Rev. B **23**, 1559 (1981).

[41] G. S. Elliot, K. E. Smith, and S. D. Kevan, Phys. Rev. B **43**, 3893 (1991).

[42] N. V. Smith, C. T. Chen, and M. Weinert, Phys. Rev. B **40**, 7565 (1989).

[43] S. G. Louie, Phys. Rev. Lett. **40**, 1525 (1978).

[44] W. Eberhardt, S. G. Louie, and E. W. Plummer, Phys. Rev. B **28**, 465 (1983).
[45] S. L. Hulbert, P. D. Johnson, and M. Weinert, Phys. Rev. B **34**, 3670 (1986).
[46] H. Conrad, M. E. Kordesch, W. Stenzel, M. Sunić, and B. Trninic-Radja, Surf. Sci. **178**, 578 (1986).
[47] J. J. Deisz, A. G. Eguiluz, and W. Hanke, Phys. Rev. Lett. **71**, 2793 (1993).